FIN BUFFET LOAD ALLEVIATION USING AN ACTIVELY CONTROLLED AUXILIARY RUDDER AT SIDESLIP

Christian Breitsamter and Boris Laschka
Lehrstuhl für Fluidmechanik, Technische Universität München
Boltzmannstrasse 15, 85748 Garching, Germany

Keywords: *Active Control, Fin Buffeting, Vortical/Unsteady Flows, High Angle of Attack*

Abstract

This investigation focuses on the efficiency of an active auxiliary rudder system in diminishing vertical tail buffeting. Low–speed wind tunnel tests are conducted on a 1/15–scale EF–2000 model representing a single–fin high–agility fighter aircraft. A specific fin model has been manufactured fitted with a computer–controlled auxiliary rudder providing harmonic oscillations. The fin is instrumented to measure the unsteady surface pressures, the fin tip accelerations and the auxiliary rudder moment. For defined rudder oscillations the surface pressure fluctuations increase with increasing frequency and deflection angle. Consequently, the root–mean–square surface pressures are shifted to higher levels even at high incidences and sideslip. It indicates that for closed–loop conditions the buffet pressures may be reduced by as much as 18 percent. Also, the rudder moment does not decrease over the incidence range regarded ($0 \div 31$ deg), thus substantiating the effectiveness of the auxiliary rudder concept. Single–input single–output control laws are employed to reduce buffeting in the first fin bending and torsion mode. The tests demonstrate that with active control fin tip acceleration spectral density peaks at the frequencies of the first eigenmodes can be reduced by as much as 60 percent up to incidences of 31 degree and even at sideslip of 5 degree.

Nomenclature

A_{F_T}	Surface area of auxiliary rudder, $0.02941\ m^2$
Can.	Canard deflection angle, $[^\circ]$
c_M	Moment coefficient
$c_p(t)$	Pressure coefficient, $(p(t)-p_\infty)/q_\infty$
$\overline{c}_p$	Time–averaged pressure coefficient
c'_p	Fluctuation part of c_p
$c_{p_{rms}}$	rms–value of c'_p, $\sqrt{\overline{c'^2_p}}$
$\hat{c}_p$	Amplitude spectrum of pressure coefficient, $\sqrt{2\,S_{c_p}\,\Delta k\,U_\infty/l_\mu}$
f	Frequency, $[Hz]$
g	Gravitational acceleration, $9.81\ m/s^2$
L.E, Tr.E.	Wing leading– and trailing–edge flap deflection, respectively, $[^\circ]$
l_μ	Wing mean aerodynamic chord, $[m]$
K_p	Controller gain parameter, $[^\circ/g]$
k	Reduced frequency, $f\,l_\mu/U_\infty$
M_{ζ_T}	Auxiliary rudder moment, $[Nm]$
$p(t)$	pressure, $[Pa]$
p_∞	ambient pressure, $[Pa]$
q_∞	freestream dynamic pressure, $[Pa]$
Re_{l_μ}	Reynolds number, $U_\infty l_\mu/\nu$
S_{c_p}	Pressure spectral density, $[1/Hz]$
$S_{F_{\ddot{y}}}$	Normalized power spectral density of fin tip accelerations
s, s_F	Wing half span, Fin span, $[m]$
s_{F_T}	Span of auxiliary rudder, $0.0656\ m$

t	Time, $[s]$
U_∞	Freestream velocity, $[m/s]$
$v'(t)$	Lateral velocity fluctuations, $[m/s]$
v_{rms}	rms value of v', $\sqrt{\overline{v'^2}}$
$\ddot{y}_F(t)$	Fin tip accelerations, $[m/s^2]$
x_F, z_F	Fin coordinates, $[m]$
α	Aircraft angle of attack, $[^\circ]$
β	Aircraft angle of sideslip, $[^\circ]$
Λ, λ	Aspect ratio, taper ratio
ν	Kinematic viscosity, $[m^2/s]$
φ	Leading–edge sweep, $[^\circ]$
Φ	Phase angle, $[^\circ]$

Subscripts

C, W, F	Canard, Wing, Fin
ζ_T	Auxiliary rudder

1 Introduction

High angle of attack and poststall maneuvers are of major interest in the design of future generation fighter aircraft [13]. Consequently, the aircraft is required to operate at high angles of attack for extended periods. Slender wing geometries, e.g. delta wing planforms, strakes, and leading–edge extensions (LEX), respectively, are used to generate strong large-scale vortices along the leading–edges. They improve significantly the high–α performance because of additional lift and an increase in maximum angle of attack [14, 3]. At high incidences, however, the vortical structure alters over the wing planform(s) called 'vortex bursting'. This bursting process is characterized by a rapid change of the vortex core flow from jet–type to wake–type associated with high turbulence intensities [3]. The corresponding unsteady aerodynamic loads often excite the natural frequencies of the aircraft vertical fin structure causing fin buffeting [16]. Especially, twin–fin configurations (F–15, F/A–18, F–22) are subject to this phenomenon because the vertical tails are directly enveloped by the highly turbulent breakdown flow [11, 15]. But single–fin configurations may also encounter severe fin buffet loads [5, 16].

In oder to analyze and reduce the buffet loads extensive research programs have been performed on scaled wind tunnel models as well as on actual aircraft in flight [9, 15, 17]. Narrow–band spectral peaks are detected on both surface pressure spectra and fin root bending moment spectra. The structural modes are driven by the flowfield dominant frequencies changing with freestream velocity and angle of attack. For a better understanding of the flow physics causing fin buffeting, comprehensive experiments on the low–speed fin flow environment of an EF–2000 model has been undertaken at the Lehrstuhl für Fluidmechanik (FLM) of the Technische Universität München (TUM) [5, 3]. The investigations concentrate on the turbulent flow structure well defined by the spatial and temporal characteristics of the unsteady flow velocities. It was detected that the flow downstream of bursting is linked to a helical mode instability. The quasi–periodic velocity fluctuations associated with the most unstable normal mode of the mean velocity profiles of the burst vortex evoke coherent unsteady surface pressures (buffet) [6]. Downstream of bursting maximum turbulence intensities are concentrated on a limited radial range related to the points of inflection in the radial profiles of the retarded axial core velocity. The flowfield surveys show that the burst vortex cores grow significantly with increasing incidence. Thus, also a center–line fin experience a higher turbulence level at high–α [5] while the fluctuation intensity raises strongly at some sideslip [8].

The buffet loads do not only decrease the fatigue life of the airframe, but may, in turn, limit the angle–of–attack envelope of the aircraft. In general, the fatigue loads may be reduced either by the reinforcement of the fin structure, by altering the fin flow characteristics to diminish the buffet loads, or by active control to alleviate the buffeting response (i.e. adding damping) or the buffet loads itself. Hence, the development and assessment of active control concepts is of great importance for existing and newly developed aircraft to reach both higher combat efficiency and an increase in the service life.

Currently, several active control methods to alleviate fin vibrations are tested in a technology program of adaptive structures for the EF–2000

aircraft [2]. The concepts comprise piezoelectric systems, like surface integrated piezoelectric actuators and a piezo interface at the interconnection of the fin to the rear fuselage, as well as aerodynamic systems, such as rudder and an auxiliary rudder device. The concept of a commanded rudder to alleviate fin buffeting was proposed 1992 by H. Ashley et al. [1]. The use of actively controlled piezoelectric actuators to reduce fin vibrations is also extensively investigated. Tests are carried out on generic wind tunnel models [12] as well as on 1/6–scale and full–scale F/A–18 models (ACROBAT–, SIDEKIC–program) [19, 18].

The experiments presented focus on the efficiency of the auxiliary rudder concept which is tested the first time using an EF–2000 wind tunnel model of 1/15–scale. Here, mainly sideslip conditions are addressed whereas investigations for symmetric flow conditions are reported in [7].

2 Measurement Technique

2.1 Model and Facility

The wind tunnel tests are performed on a detailed rigid steel model of a modern fighter aircraft of canard–delta wing type (Fig. 1). The model consists of nose section, front fuselage with rotatable canards and a single place canopy, center fuselage with delta wing section and a through–flow double air intake underneath, and rear fuselage including nozzle section and the vertical tail (fin). For the present investigations, a completely new fin section has been constructed fitted with an actively controlled auxiliary rudder. The surface models of the computer–aided design (CAD) and the main assembly parts are shown in Fig. 2.

The fabricated parts include the fin with an instrumentation cover, the active auxiliary rudder, the body insert to fasten the fin to the rear fuselage and the driving components. The auxiliary rudder is commanded via an excenter gear by a computer–controlled servo motor providing harmonic (sinusoidal) rudder motions (Fig. 3). The oscillation frequency f_{ζ_T} can be adjusted digitally while the maximum rudder deflection

$s_F = 0.47\ s$	
$\varphi_F = 54°$	
$\Lambda_F = 1.38$	
$\lambda_F = 0.19$	

$2s = 0.740$ m	$\varphi_W = 50°$
$l_\mu = 0.360$ m	$\varphi_C = 45°$
$\Lambda_W = 2.45$	$\lambda_W = 0.14$

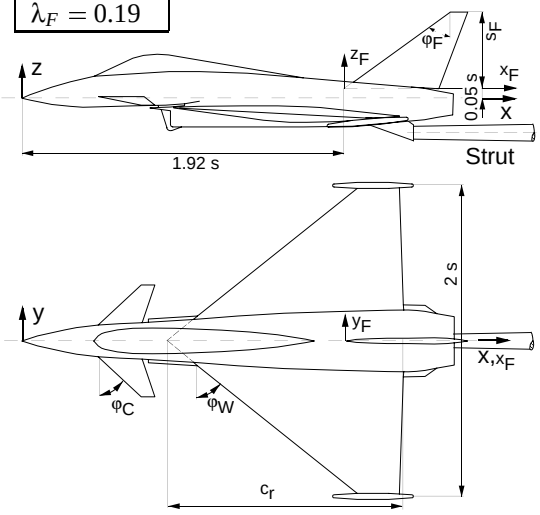

Fig. 1 Geometry of EF–2000 wind tunnel model.

angle is fixed mechanically to $\zeta_{T_{max}} = 1°, 3°, 5°$. To reduce the inertia forces acting on the auxiliary rudder its mass is only 0.015 *kg*. Thus, accelerations at the rudder tip are limited to 250 *g*

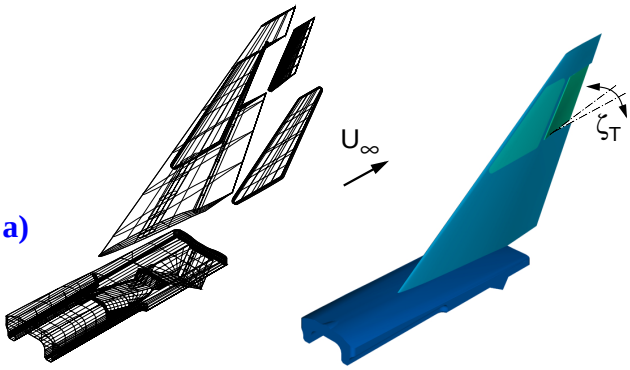

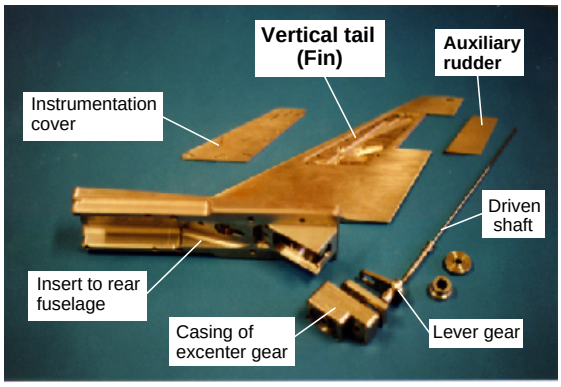

Fig. 2 Fin section components. a) CAD models, b) assembly parts with driven auxiliary rudder.

at a maximum oscillation frequency of 120 *Hz*. The fin is instrumented with 2 tip accelerometers, 18 differential unsteady pressure transducers at 9 positions directly opposite each other on each surface and a torque moment transducer at the driven rudder shaft (Fig. 3).

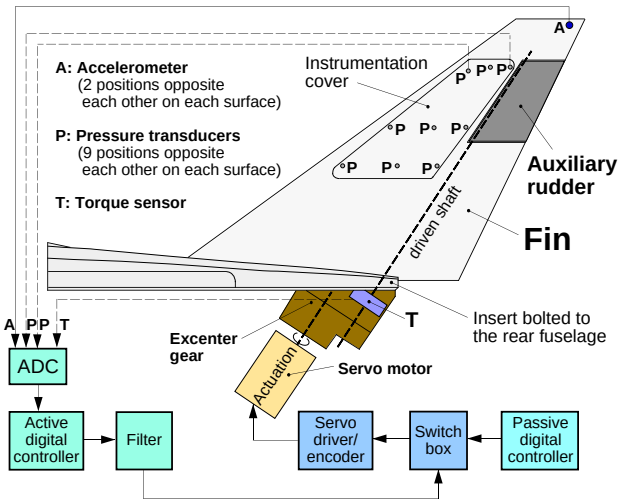

Fig. 3 Measurement and control system for fin buffet and buffeting alleviation.

The investigations were conducted in the Göttingen type low–speed wind tunnel **B** of the Lehrstuhl für Fluidmechanik of the Technische Universität München. The open test section is 1.2 *m* in height and 1.55 *m* in width and 2.8 *m* long. Maximum usable velocity is 60 m/s with a turbulence level less than 0.4%. The model is sting mounted on its lower surface by a computer–controlled three–axis model support (Fig. 4).

2.2 Test Conditions

Since active control of buffet–induced vibrations is the primary focus the first fin eigenmodes are of particular interest. At wind–off the first bending mode of the fin model is around 145 *Hz* and the first torsion mode is around 387 *Hz*. The structural damping is about 4.4%, whereas the aerodynamic damping is $3.2\% \div 4.8\%$ for $\alpha = 25^\circ \div 31.2^\circ$.

For buffet, the reduced frequency k with

$$\frac{f\, l_\mu}{U_\infty} = \frac{f_M\, l_{\mu_M}}{U_{\infty_M}} \qquad \text{M: Model} \qquad (1)$$

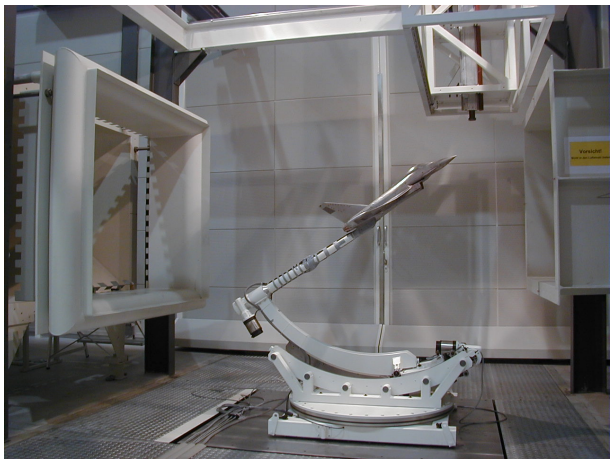

Fig. 4 EF–2000 model mounted in the FLM low–speed wind tunnel **B**.

is the basic similarity parameter in determining test conditions. The frequency ratio between the considered structural modes of the actual aircraft and the model is $1/8$. The model scale is $1/15$. With respect to low–speed, high angle–of–attack maneuvers the tests are made at a freestream reference velocity of $U_\infty = 40\ m/s$ corresponding to a Reynolds number of $Re_{l_\mu} = 0.97 \times 10^6$ based on the wing mean aerodynamic chord. The angle of attack is varied in the range of $0^\circ \leq \alpha \leq 31.2^\circ$ at sideslip angles of $\beta = 0^\circ$, and 5°. The results shown herein deals mainly with $\beta = 5^\circ$. Turbulent boundary layers are present at wing and control surfaces known from previous experiments [3].

Using a multi–channel data acquisition system, output voltages of unsteady surface pressure transducers, fin tip accelerometers and the rudder moment sensor are amplified for optimal signal levels, low–pass filtered at 256 *Hz* and 1000 *Hz*, respectively, and simultaneously sampled and digitized with 14–bit precision. The sampling rate for each channel is set to 2000 *Hz* and the sampling interval is 30 *s* [4]. The data acquisition parameters are based on preliminary tests to cover all significant flow phenomena as well as on statistical accuracies of 1, and 2.5% for the rms values and spectral densities, respectively [3].

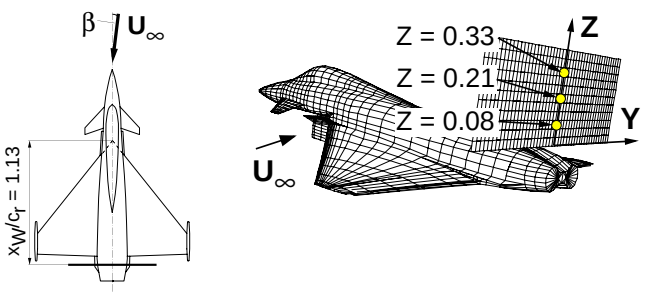

WLV : Wing leading-edge vortex
CLV : Canard leading-edge vortex
CTV : Canard trailing-edge vortex
CAV : Canopy vortex system

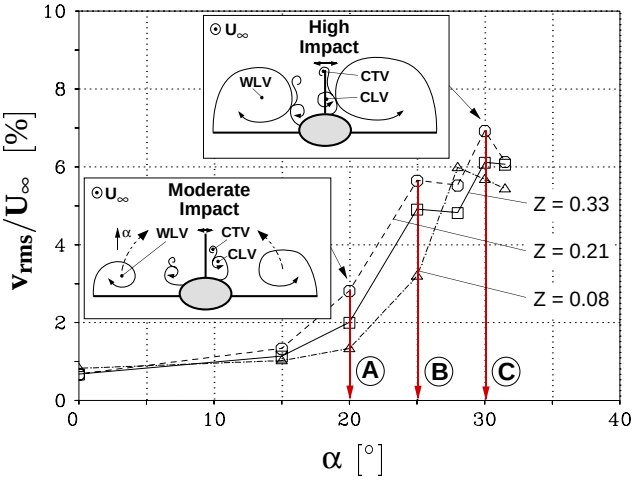

a) rms values for various vertical fin stations $Z = z_F/s$

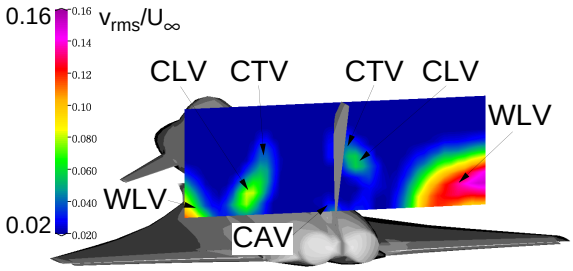

b) Plane normal to fin surface; $\alpha = \mathbf{20}^\circ$ (A)

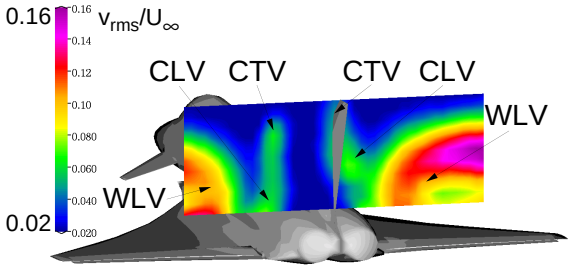

c) Plane normal to fin surface; $\alpha = \mathbf{25}^\circ$ (B)

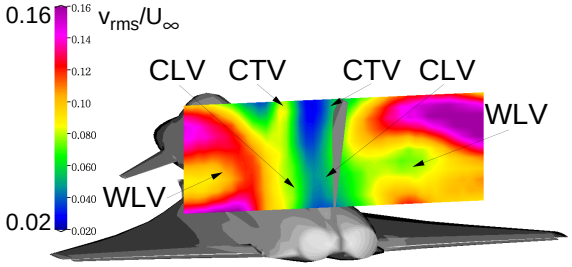

d) Plane normal to fin surface; $\alpha = \mathbf{30}^\circ$ (C)

Fig. 5 Fin lateral rms velocities v_{rms}/U_∞ as function of angle of attack at $\beta = 5^\circ$ and $Re_{l_\mu} = 0.97 \times 10^6$.

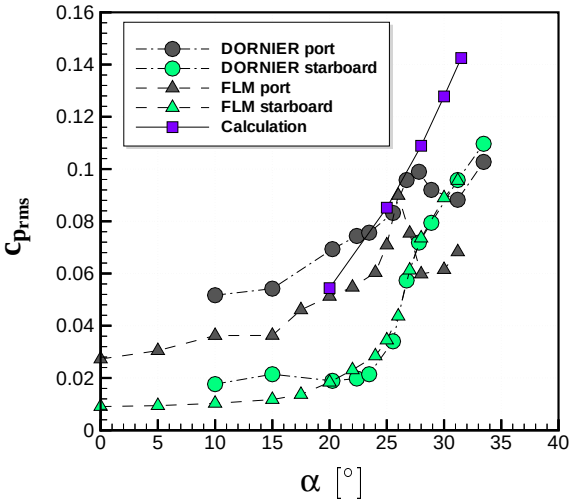

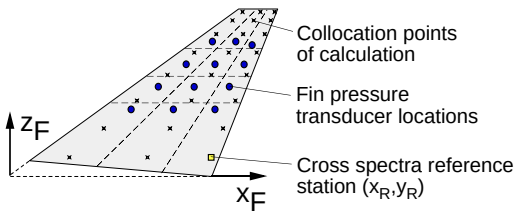

DORNIER: **12** pressure transducers at stations opposite each other on each surface

FLM: **9** pressure transducers at stations opposite each other on each surface

Calculation: $\mathbf{3} \times \mathbf{8}$ measurement/collocation points

Fig. 6 Measured and calculated fin buffet pressure as function of angle of attack at $\beta = 5^\circ$. DORNIER: $\mathbf{Ma} = \mathbf{0.5}$, $\mathbf{Re}_{l_\mu} = \mathbf{3.01} \times \mathbf{10^6}$, Can. $= -\mathbf{10}^\circ$, L.E. $= -\mathbf{20}^\circ$, Tr.E. $= +\mathbf{20}^\circ$ [3]; FLM & Calculation: $\mathbf{Ma} = \mathbf{0.12}$, $\mathbf{Re}_{l_\mu} = \mathbf{0.97} \times \mathbf{10^6}$, Can. $= \mathbf{0}^\circ$, L.E. $= \mathbf{0}^\circ$, Tr.E. $= \mathbf{0}^\circ$ [3, 6] .

3 Buffet and Buffeting Characteristics

The vortical flowfields causing fin buffeting have been extensively analyzed carrying out tests on generic wind tunnel models as well as on the EF–2000 model. The velocity fluctuations are measured in detail in the fin region to quantify the buffet excitation level. For a single–fin mainly the lateral turbulence intensity causes buffeting [6]. Here, the lateral rms values are documented for different vertical fin stations as function of angle of attack (Fig. 5a). The rms levels depend on the evolution of the vortex systems illustrated by the schematics of Fig. 5a. The sketches are derived from the rms velocity patterns of planes normal to the fin surface (Figs. 5b-d). At sideslip, $\beta = 5^\circ$, the starboard vortices are shifted inboard and upward while the port one's are moved outboard and downward. At $\alpha = 20^\circ$, the burst starboard canard vortices emanating from the leading– and trailing–edge (CLV, CTV) are located near the plane of symmetry together with a vortex pair (CAV) shed at the canopy (Fig. 5b). The corresponding local turbulence maxima evoke rms values in the midsection which have increased to three times the level of symmetric flow conditions [7]. With increasing angle of attack the burst wing leading–edge vortices (WLVs) move inboard and upward while their core regions expand rapidly (Fig. 5c). Therefore, the annular regions of maximum turbulence intensity come close to the midsection leading to a significant increase of lateral rms velocity at the fin. In particular, the starboard WLV sheets produce a highly turbulent flow at the fin tip (Fig. 5d).

The related surface pressure fluctuations defining the buffet situation are averaged for each side of the fin and plotted together as function of angle of attack (Fig. 6). The buffet pressures increase strongly above $\alpha = 20^\circ$ reflecting the rise in the lateral rms velocities. Flow separation on the port side of the fin leads to a rms drop at $\alpha \approx 27^\circ$. The results are taken from unsteady pressure measurements on different models of 1/15–scale (DORNIER 1989 [3]; FLM 1998 [4]) as well as from pressure calculations based on measured turbulent flowfields [6]. The data obtained depict a good agreement over the incidence range regarded.

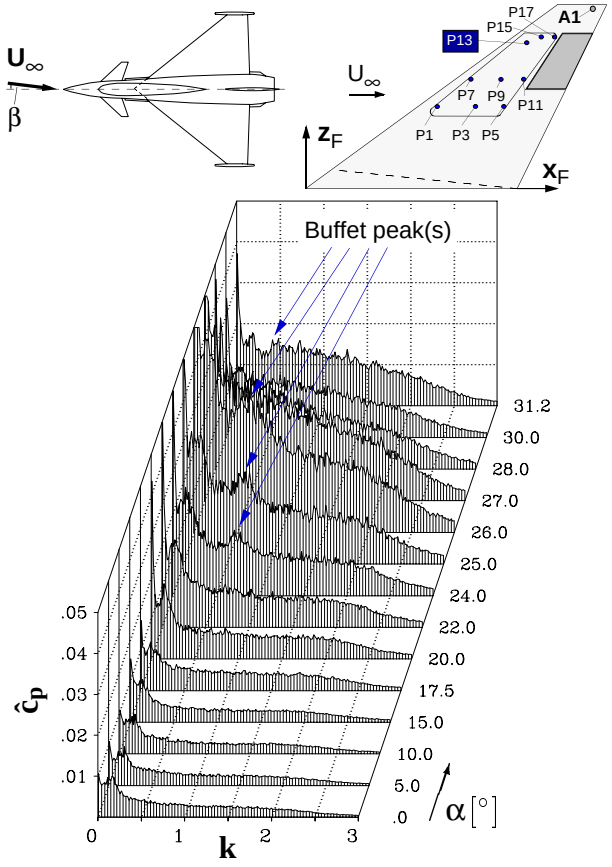

Fig. 7 Amplitude spectra of fluctuating fin surface pressures $\hat{c}_p$ at station P13 for various angles of attack at $\beta = 5^\circ$. $U_\infty = 40\ m/s$, $Re_{l_\mu} = 0.97 \times 10^6$.

For further analysis, nondimensional spectral functions are used to evaluate buffet and buffeting. Above $\alpha \approx 22^\circ$ surface pressure spectra exhibit distinct peaks indicating that turbulent energy is channeled into a narrow band (Fig. 7). At this α the helical mode instability of the WLV breakdown flow starts to influence the fin pressure field. With increasing angle of attack the amplitude values of the quasi–periodic oscillations increase significantly while the dominant reduced frequencies decrease. This change in reduced frequency is due to the growth of the wave lengths of the narrow–band fluctuations with angle of attack. A scaling with the sinus of α gives an ap-

proximately constant value [7] of

$$k_{dom} \sin\alpha \approx 0.335 \pm 0.025 . \qquad (2)$$

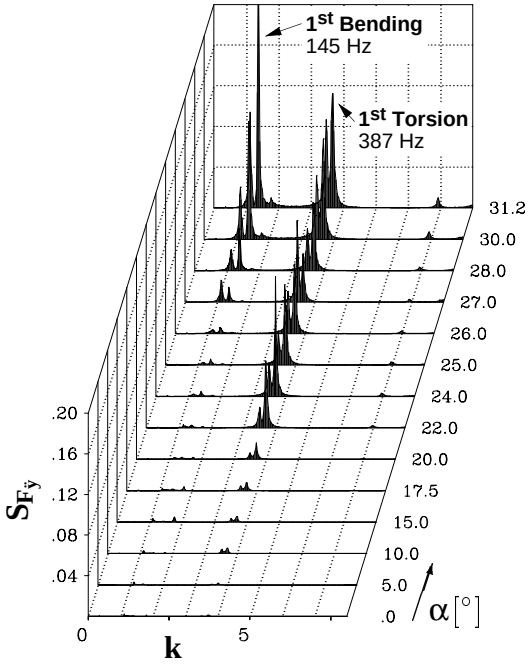

Fig. 8 PSDs of fin tip accelerations $S_{F_{\dot{y}}}$ for various angles of attack at $\beta = 5°$. $Re_{l_\mu} = 0.97 \times 10^6$.

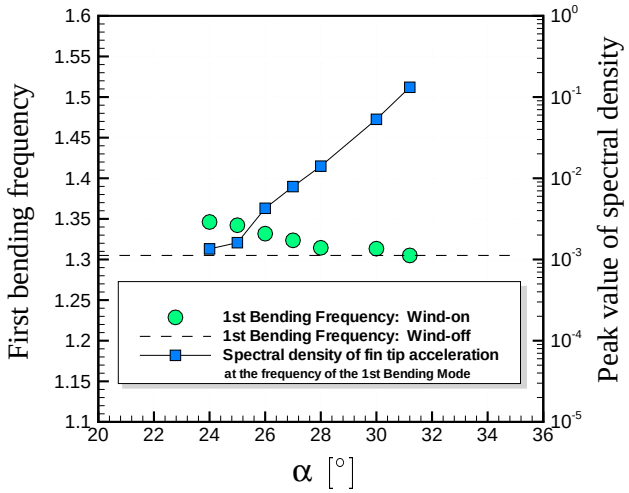

Fig. 9 First fin bending frequency and assigned PSD peak values as function of angle of attack.

The pressure distributions discussed (Figs. 6, 7) create the buffeting, or structural response to the buffet, typically quantified by power spectral densities (PSDs) of the fin tip accelerations (Fig. 8). The resulting fin buffeting mainly consists of a response in the first bending and torsion mode. At high incidence, the dominant buffet frequency comes close to a value half of the bending eigenfrequency which is then strongly excited whereas the first torsion mode with a multiple higher eigenfrequency is less excited. Analyzing the spectra a gradual shift in the frequency of the first bending mode with angle of attack is found while the logarithmic growth of the amplitude values is nearly linear (Fig. 9). This shift in frequency may be seen as increases in aerodynamic damping regarding the fin as a single degree–of–freedom system excited by the large narrow–band perturbations of the breakdown flow.

4 Open–Loop Experiments

Harmonic rudder motions at varying frequency f_{ζ_T} and maximum deflection angles $\zeta_{T_{max}}$ of 1°, 3°, and 5° are carried out to assess the auxiliary rudder efficiency in altering buffet and buffeting. Compared to the results of the fixed or stationary deflected rudder, the oscillating rudder shifts the rms values of the surface pressure fluctuations to higher levels (Fig. 10). The motion induced unsteady pressures increase both with rudder frequency and with rudder deflection angle even at high incidences and sideslip. Because of partially separated flow on the leeward side the rms shift is there slightly lower than on the windward side. It proves that the auxiliary rudder has the potentiality to diminish the rms levels of the buffet pressure fluctuations by as much as 16% to 18%.

The pressure spectra depict narrow–band distributions with a buffet peak, evoked by the quasi–periodic fluctuations of the breakdown flow, which is similar to the case with stationary rudder (Fig. 11). In addition, spikes are found at the values of the auxiliary rudder frequencies indicating that at these frequencies the fluctuating pressure field is feeded with energy. The spike amplitudes remain approximately the same for all incidences tested demonstrating again that the active auxiliary rudder is efficient to alleviate the buffet loads.

Furthermore, amplitude and phase angle of the rudder moment coefficient $c_{M_{\zeta_T}}$ are evaluated

(Fig. 12). Dynamic freestream pressure q_∞ and the surface area A_{F_T} and span s_{F_T} of the auxiliary rudder are used to calculate the moment coefficient, Eq. (3).

$$c_{M_{\zeta_T}} = \frac{M_{\zeta_T}}{q_\infty A_{F_T} s_{F_T}} \qquad (3)$$

It is shown that the amplitude of the rudder moment is nearly constant over the considered incidence range. It substantiates that there is no reduction of the auxiliary rudder effectiveness at high–α while the phase angle of the auxiliary rudder moment with respect to the commanded motion is in the range of $-20^\circ \div -40^\circ$.

5 System Identification and Active Control

5.1 Transfer function

The open–loop frequency response function between the commanded auxiliary rudder deflection angle and the fin tip accelerations (Fig. 13) is the input–output relationship of the forward loop of the active control system (Fig. 14). The transfer functions obtained are based on a linear frequency sweep of $k = 0 \div 0.81$ with the rudder driven harmonically at $\zeta_{T_{max}} = 1^\circ$, 3°, and 5°. To concentrate mainly on the first fin bending

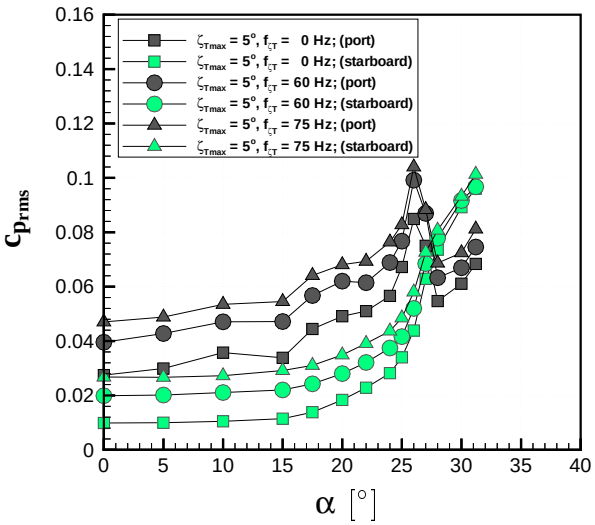

Fig. 10 rms fin surface pressure (averaged for each side of the fin) as function of angle of attack at oscillating rudder and $\beta = 5^\circ$. $Re_{l_\mu} = 0.97 \times 10^6$.

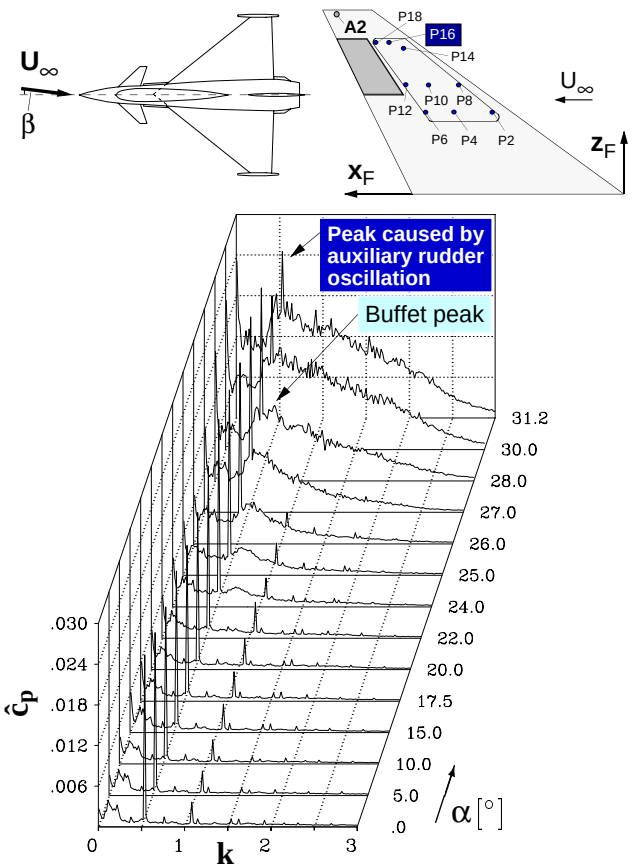

a) $k_{\zeta_T} = f_{\zeta_T}\, l_\mu / U_\infty = 0.540$, $\zeta_{T_{max}} = 3^\circ$

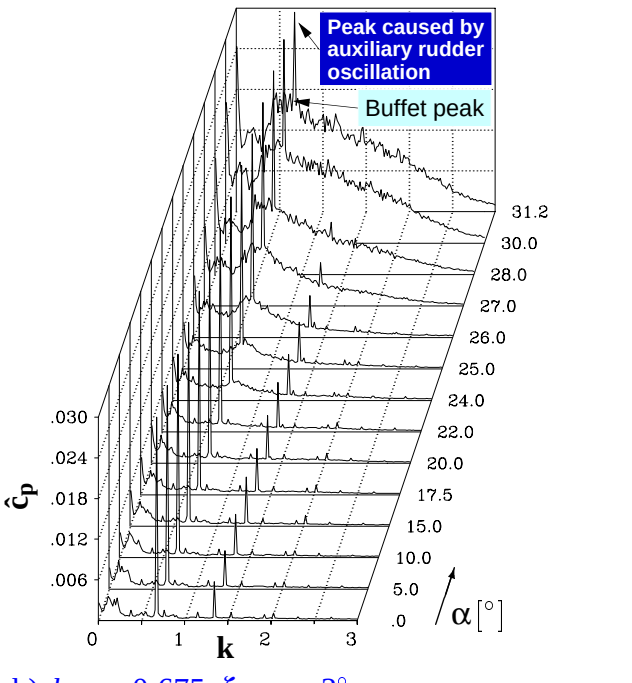

b) $k_{\zeta_T} = 0.675$, $\zeta_{T_{max}} = 3^\circ$

Fig. 11 Amplitude spectra of fluctuating fin surface pressures $\hat{c}_p$ at station P16 for various angles of attack at $\beta = 5^\circ$. $U_\infty = 40\ m/s$, $Re_{l_\mu} = 0.97 \times 10^6$.

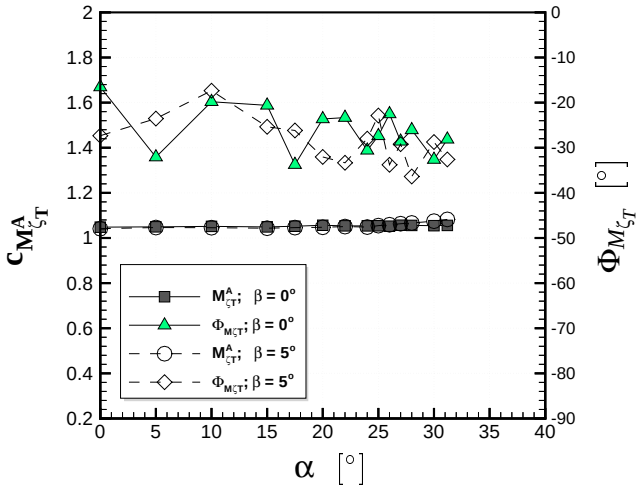

Fig. 12 Amplitude $c_{M^A_{\zeta_T}}$ and phase angle $\Phi_{M_{\zeta_T}}$ of the auxiliary rudder moment coefficient at $k_{\zeta_T} = 0.675$ and $\zeta_{T_{max}} = 3°$ as function of angle of attack and sideslip $\beta = 0°$, and $5°$. $Re_{l_\mu} = 0.97 \times 10^6$.

mode the frequency sweep is limited to $k = 0.81$ (90 Hz). The resonance case producing maximum fin tip accelerations is achieved when the rudder oscillates with a frequency of $k = 0.623$ (72.5 Hz) which is half the bending eigenfrequency. The logarithmically scaled amplitude spectrum of the transfer function shows a nearly linear rise to the peak value at the frequency of the first bending mode (Fig. 12a) while the corresponding phase angle varies between $\pm 180°$ (Fig. 12b). Since the buffet induced vibrations contribute to the response of the vertical fin, the open–loop frequency response functions are measured for wind–off and wind–on conditions at various α.

5.2 Control Law Development

The active control system consists of an analog–to–digital (A/D) converter, a digital controller in which the control law is implemented, and a digital–to–analog (D/A) converter connected with amplifier and filter components to run the actuator and the servo motor, respectively (Fig. 14a). The control laws employed are based on frequency domain compensation methods [10] using the experimentally derived open–loop frequency response functions. Single–input single–output relationships are applied with the fin tip accelerometers as sensors to reduce the response in the first fin bending and torsion mode, respectively. The commanded rudder motion may provide damping to alleviate the buffeting of the fin by lagging accelerations by ninety degrees of phase. Therefore, the baseline control laws are designed to subtract phase at the frequencies of the first eigenmodes that the actuator phase lags fin tip accelerations by ninety degrees (Fig. 14b). The control law design considers also phase lags asso-

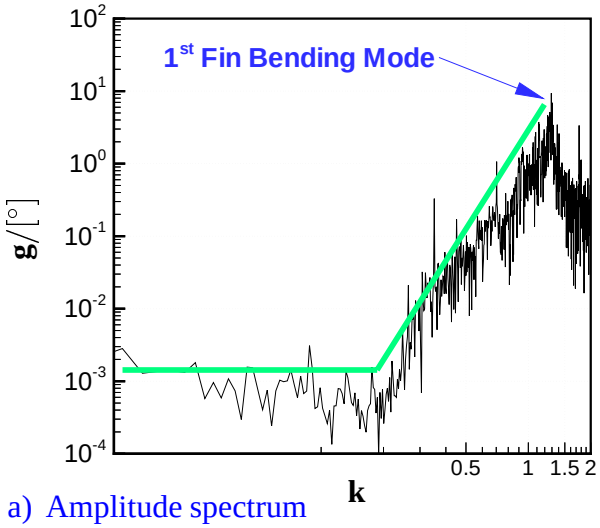

a) Amplitude spectrum

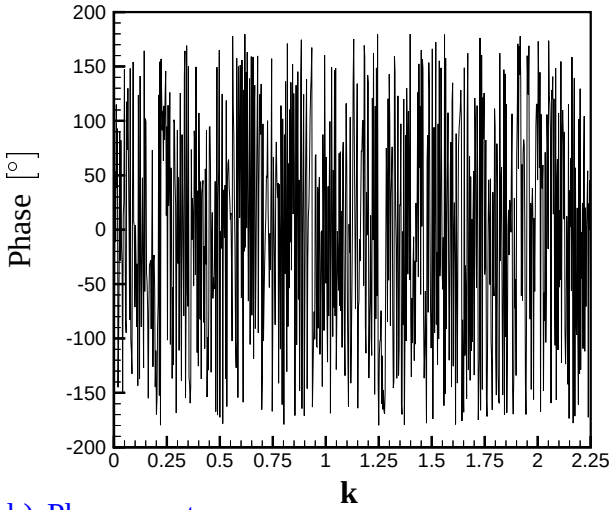

b) Phase spectrum

Fig. 13 Open–loop frequency response function of fin tip accelerations vs. commanded auxiliary rudder oscillations for a frequency sweep of $k = 0 \div 0.81$ at wind–on ($U_\infty = 40\ m/s$) and $\alpha = 0°$.

ciated with time delays caused by the digital signal processing, especially the digital controller, as well as the actuator motion. Consequently, the phase relation of the control law may be modified by a zero order hold to take these delays into account [10]. To avoid the excitation of higher frequency modes sufficient filtering is needed decreasing the control law gain beyond $k = 0.75$. Furthermore, it is assumed that there is no markable change in the phase relationship between fin tip accelerations and commanded rudder motions with the angle of attack. Regarding the fin as a single degree–of–freedom system extensive numerical controller simulations are conducted to prove the efficiency of the baseline control laws [7]. Stability gain margins are computed to ensure that the control law will not produce any instabilities.

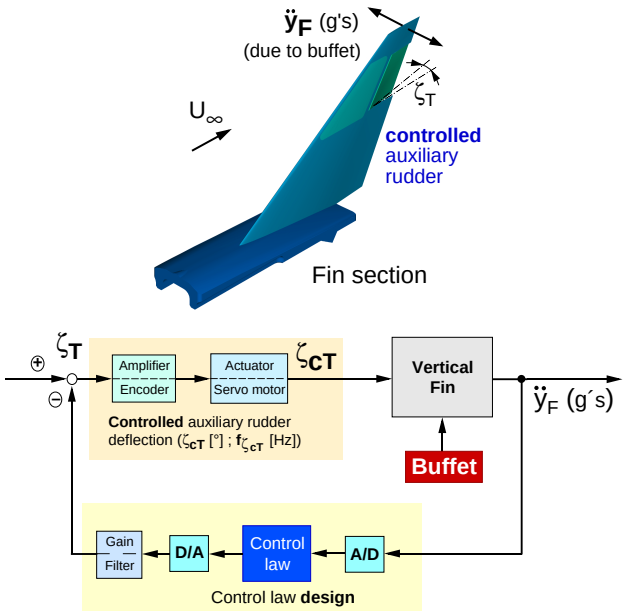

a) Control system

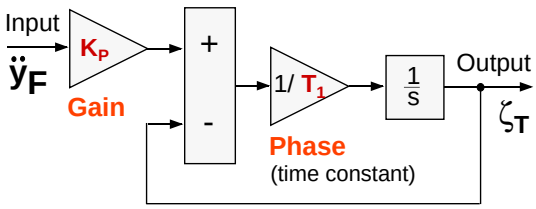

b) Control law schematic

Fig. 14 Active control system.

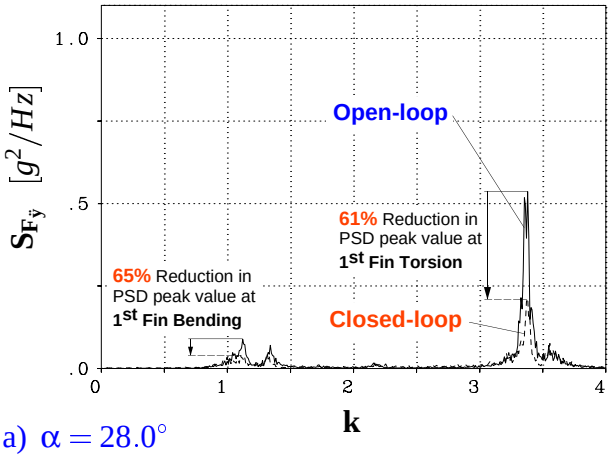

a) $\alpha = 28.0°$

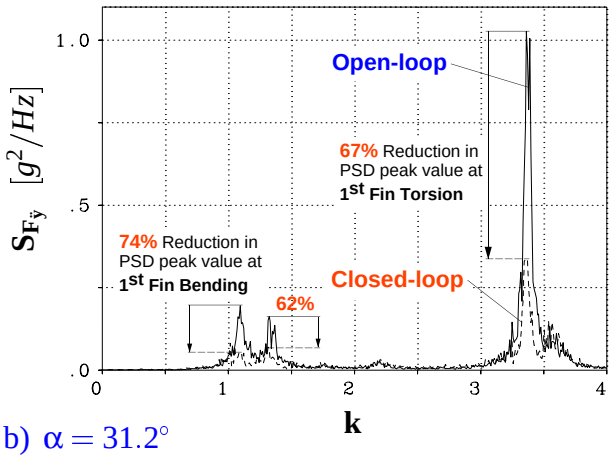

b) $\alpha = 31.2°$

Fig. 15 Comparison of fin tip acceleration PSD's without and with active auxiliary rudder control at various α and $\beta = 5°$. $Re_{l_\mu} = 0.97 \times 10^6$.

5.3 Active Buffeting Alleviation

The PSD results of the open–loop and closed–loop wind tunnel experiments demonstrate that with active auxiliary rudder control a substantial decrease of the fin tip accelerations referring to the first bending and torsion mode is achieved (Fig. 15). The commanded rudder motions reduce the corresponding PSD peak values by as much as 61% to 74%. This reduction in the structural response is obtained at gain factors well below the physical limit of the rudder driving system. For these tests, a constant gain factor was used over the incidence range of interest.

The PSD peak values of the open–loop and closed–loop tests concerning the first fin bending mode are summarized in Fig. 16 to illustrate the

buffeting reduction as function of angle of attack. It is shown that with active control the structural dynamic loads are significantly lower indicating a decrease in the PSD peak value of at least 60% at all angles of attack investigated. It is supposed that a further improvement in the closed–loop response can be obtained by raising the gain factor in the control law within the stability region without driving the first fin bending or torsion mode, to increase the percentage of total damping added to the system by using active control. In addition, pressure transducers may be used as sensors to quantify how the buffet loads themselves are actively influenced by the controlled rudder deflections.

6 Conclusions and Outlook

Experimental investigations have been conducted on an EF–2000 model to study aerodynamic active control in reducing single–fin buffeting. The focus is on the effectiveness of a commanded auxiliary rudder in altering buffet pressures and reducing vibrations in the first fin bending and torsion mode. A new fin model featuring an active auxiliary rudder has been manufactured and instrumented to measure unsteady surface pressures, fin tip accelerations and the transient rudder momemt. The auxiliary rudder oscillates harmonically driven by a computer–controlled servo motor via an excenter gear. The rudder efficiency is demonstrated by wind tunnel tests varying rudder frequency and maximum deflection angle at incidences up to 31° and sideslip of 5°. The control laws are based on frequency domain compensation methods using the measured open–loop frequency response functions to alleviate the buffeting of the fin.

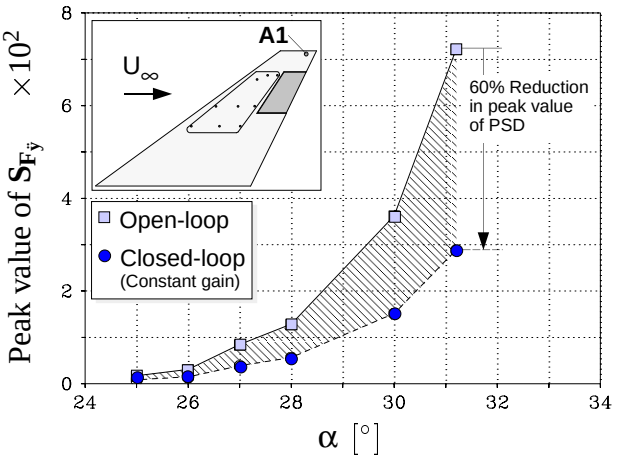

Fig. 16 Comparison of the fin tip acceleration PSD peak values (station A1) at the frequency of the first bending mode for open–loop and closed–loop conditions. $U_\infty = 40\ m/s$, $Re_{l_\mu} = 0.97 \times 10^6$.

These investigations show the following major results:

1. The fin surface pressure fluctuations raise with increasing rudder frequency and deflection angle at oscillating auxiliary rudder. The corresponding rms values exhibit higher levels even at high angles of attack and sideslip compared to the case with non–oscillating rudder. Closing the loop the buffet pressures may be reduced by as much as 18 percent.

2. The amplitude of the rudder moment does not decrease with increasing angle of attack while the phase angle takes on values of about −30°. It substantiates that the auxiliary rudder works also effectively in the high–α regime.

3. Single–input single–output control laws are successfully employed to diminish vibrations (buffeting) in the first fin bending and torsion mode, respectively. A constant gain factor well below the physical limits of the rudder driving system gives satisfactory results at all angles of attack tested.

4. The active control tests show that the peak value of the fin tip acceleration PSDs at the frequency of the first bending and torsion mode can be reduced by at least 60 percent at angles of attack up to 31° and sideslip of 5°.

The wind tunnel tests reported herein are the first demonstration of fin buffeting alleviation on an EF–2000 model at sideslip using an active auxiliary rudder. Further improvements in buffeting

alleviation may result from control law modifications to raise the control law gain factor within the stability region. Adaptive control methods using parameters which depend on the angle of attack may also enhance the system performance in buffeting reduction.

Acknowledgment

This work was supported by the DaimlerChrysler Aerospace AG (Military Aircraft Division, DASA–M). The authors would like to thank Dr.-Ing. J. Becker (DASA–M) for his kind assistance.

References

[1] Ashley H, Rock S. M, Digumarthi R. V, Chaney K, and Eggers, Jr. A. J. *Active Control for Fin Buffet Alleviation*. WL–TR–93–3099, Wright Patterson AFB, OH, Jan. 1994.

[2] Becker J and Luber W. Comparison of Piezoelectric and Aerodynamic Systems for Aircraft Vibration Alleviation. *Proc SPIE 5th Annual Symposium on Smart Structures and Materials, Conf. Paper 3326–04*, pp 1–15, San Diego (CA), USA, March, 1998.

[3] Breitsamter C. *Turbulente Strömungsstrukturen an Flugzeugkonfigurationen mit Vorderkantenwirbeln*. Dissertation, Technische Universität München, Herbert Utz Verlag, 1997.

[4] Breitsamter C. Aerodynamic Active Vibration Control For Single–Fin Buffeting Alleviation. *Proc Deutscher Luft– und Raunfahrtkongress/ DGLR–Jahrestagung*, Vol. I, pp 291–300, Berlin, Germany, Sept., 1999.

[5] Breitsamter C and Laschka B. Turbulent Flow Structure Associated with Vortex–Induced Fin Buffeting. *Journal of Aircraft*, Vol. 31, No 4, pp 773–781, 1994.

[6] Breitsamter C and Laschka B. Fin Buffet Pressure Evaluation Based on Measured Flowfield Velocities. *Journal of Aircraft*, Vol. 35, No 5, pp 806–815, 1998.

[7] Breitsamter C and Laschka B. Aerodynamic Active Control For EF–2000 Fin Buffet Load Alleviation. *Proc 38th Aerospace Sciences Meeting and Exhibit, AIAA Paper 2000–0656*, pp 1–11, Reno (NV), USA, Jan., 2000.

[8] Breitsamter C and Laschka B. Turbulent Flowfield Structure Associated to Fin Buffeting Around a Vortex–Dominated Aircraft Configuration at Sideslip. *Proc 19th Congress of the International Council of the Aeronautical Sciences, ICAS–94–4.3.1*, Vol. 1, pp 768–784, Anaheim (CA), USA, Sept., 1994.

[9] Ferman M. A, Patel S. R, Zimmermann N. H, and Gerstenkorn G. A Unified Approach to Buffet Response of Fighter Aircraft Empennage. *Proc Aircraft Dynamic Loads due to Flow Separation, AGARD–CP–483*, pp 2–1–2–18, Sorrento, Italy, April, 1990.

[10] Franklin G. F, Powel J. D, and Emami-Naeini A. *Feedback Control of Dynamic Systems*. Addison–Wesley Publishing Company, Reading MA, 1986.

[11] Frate J. H. D and Zuniga F. A. In–Flight Flow Field Analysis On the NASA F–18 High Alpha Research Vehicle With Comparisons to Ground Facility Data. *Proc 28th Aerospace Sciences Meeting, AIAA Paper 90–0231*, pp 1–26, Reno (NV), USA, Jan., 1990.

[12] Hauch R. M, Jacobs J. H, Dima C, and Ravindra K. Reduction of Vertical Tail Buffet Response Using Active Control. *Journal of Aircraft*, Vol. 33, No 3, pp 617–622, 1996.

[13] Herbst W. B. Future Fighter Technologies. *Journal of Aircraft*, Vol. 17, No 8, pp 561–566, 1980.

[14] Hummel D. Documentation of Separated Flows for Computational Fluid Dynamics Validation. *Proc Validation of Computational Fluid Dynamics, AGARD–CP–437*, Vol. 2, pp 18–1–18–24, Lisbon, Portugal, April, 1988.

[15] Lee B. H. K, Brown D, Zgela M, and Poirel D. Wind Tunnel Investigations and Flight Tests of Tail Buffet on the CF–18 Aircraft. *Proc Aircraft Dynamic Loads due to Flow Separation, AGARD–CP–483*, pp 1–1–1–26, Sorrento, Italy, April, 1990.

[16] Luber W, Becker J, and Sensburg O. The Impact of Dynamic Loads on the Design of Military Aircraft. *Proc Loads and Requirements for Military Aircraft, AGARD–R–815*, pp 8–1–8–27, Florence, Italy, Sept., 1996.

[17] Meyn L. A and James K. D. Full–Scale Wind Tunnel Studies of F/A–18 Tail Buffet. *Journal*

of Aircraft, Vol. 33, No 3, pp 589–595, 1996.

[18] Moses R. W. Contributions to Active Buffeting Alleviation Programs by the NASA Langley Research Center. *Proc 40th AIAA/ASME/ASCE/ AHS/ASC Structures, Structural, and Materials Conference, AIAA Paper 99–1318*, pp 1–9, St. Louis (MO), USA, April, 1999.

[19] Moses R. W. Vertical Tail Buffeting Alleviation Using Piezoelectric Actuators – Some Results of the Actively Controlled Response of Buffet–Affected Tails (ACROBAT) Program . *Proc SPIE 4th Annual Symposium on Smart Structures and Materials, Conf. 3044*, pp 1–12, San Diego (CA), USA, March, 1997.